Environmental Earth Sciences (2021) 80:396
https://doi.org/10.1007/s12665-021-09704-5

ORIGINAL ARTICLE

Mining subsidence monitoring model based on BPM-EKTF and TLS and its application in building mining damage assessment

JingYu Li[1,2,4] · Lei Wang[1,2,3,4]

Received: 8 February 2021 / Accepted: 12 May 2021 / Published online: 23 May 2021

Abstract

In mining subsidence monitoring, "discrete point deformation monitoring and mining subsidence prediction model" is often used. The key to mining subsidence monitoring is to choose a convenient, economical, accurate, and reliable deformation monitoring method. In this study, the terrestrial laser scanner (TLS) with convenient, high efficiency, and high precision was used as the data acquisition method. And the Boltzmann function prediction method-exponent Knothe time function mining subsidence prediction model with high simulation degree for the deformation of rock strata above the mining affected area was constructed to calculate the surface deformation. Taking the surrounding area of South 1312 (1) working face of Gubei Coal Mine in Huainan, China as the application area, first, the model parameters are obtained by the wolf pack algorithm according to the TLS scanning point cloud data, followed by predicting the subsidence and horizontal displacement of the surrounding area. Finally, the building mining damage assessment is conducted according to the deformation of the surrounding area of the working face. The analysis results show that the mining subsidence monitoring method proposed in this paper can obtain the surface deformation in a large area affected by mining after observing a small area. The surface deformation obtained by this method is consistent with the surface deformation obtained by leveling observation. Moreover, the predicted effect of this method is better than that of the mining subsidence monitoring method using PIM-KTF model combined with TLS, and it has certain robustness to the geological and mining condition errors. The results of this work can provide a reference for predicting mining subsidence influence scope, deformation size, and mining damage assessment of mining buildings.

Keywords Mining subsidence monitoring · Terrestrial laser scanner · Boltzmann function · Exponent Knothe time function · Mining damage assessment · Wolf pack algorithm

Introduction

The energy resource structure of China has the characteristics of "rich in coal, poor in oil, and little in gas." The production and consumption of coal resources in the primary energy structure accounted for 76% and 66%, respectively. Therefore, before the scale of renewable resources is formed, coal was the primary energy source for a long time, shouldering the important task of energy security and sustainable economic development (Yuan et al. 2018). High-intensity coal mining is bound to cause environmental disasters in mining areas, such as surface collapse and engineering geological damage (Wang and Xiong 2020). Mining subsidence monitoring can play a guiding role in coal mining and environmental disaster prevention in mining areas (Zeng et al. 2020; Jiang et al. 2021; Xiao et al. 2021). Therefore, monitoring mining subsidence has always gained significant attention in China's mining field (Liu et al. 2019; Kumar et al. 2020).

✉ Lei Wang
austwlei@163.com

1 State Key Laboratory of Mining Response and Disaster Prevention and Control in Deep Coal Mines, Anhui University of Science and Technology, Huainan 232001, China

2 School of Geodesy and Geomatics, Anhui University of Science and Technology, Huainan 232001, China

3 Jiangsu Key Laboratory of Resources and Environmental Information Engineering, China University of Mining and Technology, Xuzhou 221116, Jiangsu, China

4 Key Laboratory of Aviation-Aerospace-Ground Cooperative Monitoring and Early Warning of Coal Mining-Induced Disasters of Anhui Higher Education Institutes, Huainan 232001, China

Mining subsidence monitoring is often performed using "discrete point deformation monitoring and mining subsidence model prediction" (Cwiakala et al. 2020; Yao et al. 2021). Usually, two leveling observation lines are laid along the trend and tendency of the working face before coal seam mining. In the mining process of the working face, the leveling of the observation station is conducted regularly to obtain the surface deformation caused by mining. Then, combined with the mining subsidence prediction model, the parameters of the prediction model are solved, and the deformation of any point on the surface is obtained. However, the mining subsidence monitoring pose the following challenges: (1) the traditional surface deformation monitoring technology (such as leveling observation) can obtain surface deformation information, but the layout of the control network, preservation of the observation station, and subsequent monitoring can easily consume a considerable amount of manpower and material resources. (2) Mining subsidence is a complex and gradual process of surface deformation (Zhu et al. 2019). At home and abroad, the static prediction method is usually combined with the corresponding time function to achieve a dynamic prediction (Wang et al. 2018; Xing et al. 2021). It is a considerable problem to select the appropriate static prediction method to obtain the final deformation and the appropriate time function to describe the surface deformation process.

This study uses a ground laser scanner (TLS) to obtain the surface deformation (Li et al. 2019; Bonneau et al. 2020; Wojtkowska et al. 2021) specified in problem (1). As a new observation technology, the TLS has the advantages of high precision, automation, noncontact, and all-weather observation (Li et al. 2020a, b; Vos et al. 2020). The laser point cloud, whose coordinates are located in the geodetic coordinate system, can be obtained quickly, with a certain accuracy, using GPS and target balls. Because of its fast-scanning speed and high-density point cloud, the same name points can be found in the two phases of TLS scanning point cloud data and the surface deformation can then be extracted. Problem (2) is solved using the Boltzmann function prediction method (BPM) (Wang et al. 2013) to obtain the final surface deformation caused by coal mining. It uses the exponent Knothe time function (EKTF) (Chang and Wang 2003) to describe the surface subsidence process. The BPM takes the Boltzmann function as the influence function and obtains the surface deformation calculation formula according to the deduction principle and process of the probability integral method (PIM) (a relatively mature theory and widely used static prediction method of mining subsidence in China). Numerous studies have shown that the BPM can better predict the final surface deformation caused by the mining face, and the prediction result of the BPM at the edge of the subsidence basin is better than that of the PIM. EKTF is based on the hypothesis of the Knothe time function (KTF), which is a time function proposed by Polish scholar, Knothe (Malinowska et al. 2020), and widely used to describe the surface subsidence process of mining areas. An index is added to the KTF to control the change in the surface subsidence speed and acceleration. When compared with KTF, EKTF has only one more variable, but it can appropriately describe the law of surface subsidence.

Therefore, this study uses TLS to obtain the measured data and the BPM-EKTF mining subsidence prediction model to describe the surface deformation caused by mining. After extracting discrete subsidence and horizontal displacement based on the TLS scanning point cloud data, the parameters of the BPM-EKTF mining subsidence prediction model were calculated using wolf pack algorithm. Then, the subsidence and horizontal displacement of the surrounding area were predicted. Finally, according to the surface deformation prediction results, the mining damage assessment of buildings in the surrounding area was conducted.

The main contributions of this study are as follows: (1) A construction method of the static prediction method and the time function is proposed. This method divides the rectangular working face into single-day mining faces. By accumulate the deformation caused to the ground at the same time by the single-day mining faces mined at different times, the surface deformation in the process of subsidence is obtained. (2) A mining subsidence monitoring method combining BPM-EKTF and TLS was proposed. This method is based on the TLS point cloud data in a small range, and makes full use of point, line/cylinder features to extract deformation. When combined with the BPM-EKTF mining subsidence prediction model, a large range of surface deformation is obtained.

The reminder of the rest of this paper is organized as follows: "Introduction" focuses on the method of construction and parameter solving about BPM-EKTF mining subsidence prediction model. "BPM-EKTF mining subsidence prediction model" introduces the application process of mining subsidence monitoring method based on the BPM-EKTF and TLS. "Application flow of mining subsidence monitoring model" introduces the application area and data acquisition, and explains the surface deformation extraction scheme. In "Area and data of application", the model parameters are solved, and the deformation is predicted and the mining damage of building is evaluated. "Results and analysis of application" compares the BPM-EKTF and PIM-KTF mining subsidence prediction model combined with the TLS for mining subsidence monitoring, as well as the resistance of mining subsidence monitoring method in this paper to geological and mining condition errors.

BPM-EKTF mining subsidence prediction model

Theoretical basis

Boltzmann function prediction method

The Boltzmann function (Boscarino et al. 2021; Monmarche 2021) is widely used in many fields. It is found that the curve shape of the Boltzmann function is S-shaped, which is similar to the subsidence curve of the main section of the surface deformation basin in semi-infinite mining. Based on the Boltzmann function, the subsidence prediction equation of the main section of the surface deformation basin in semi-infinite mining is as follows:

$$W(x) = \frac{W_0}{1 + e^{-(x-s)/R}}, \tag{1}$$

where $W_0 = mq\cos\alpha$; m, q, α, x, S, and R represent the average mining thickness of the working face, subsidence coefficient, inclination of the working face, position of the point on the main section, inflection point displacement, and main influence radius, respectively.

By differentiating Eq. (1), the unit influence equation of the BPM can be obtained as:

$$W_e(x) = dW(x) = \frac{1}{R}\frac{e^{-x/R}}{(1 + e^{-x/R})^2}. \tag{2}$$

Following the deduction experience of the PIM and the knowledge of elasticity, the horizontal displacement equation of the element is obtained as follows:

$$U_e(x) = B\frac{dW_e(x)}{dx}, \tag{3}$$

where B denotes the coefficient of horizontal displacement.

By integrating the horizontal displacement equation of the element, the horizontal displacement of the surface point along the *x method* can be obtained as follows:

$$U(x) = W_0\frac{B}{R}\frac{e^{-x/R}}{(1 + e^{-x/R})^2}. \tag{4}$$

Accordingly, the calculation equations for the subsidence and horizontal displacement of the main section of the trend and tendency in finite mining are as follows:

$$\begin{cases} W^0(x) = W(x) - W(x-l) \\ U^0(x) = U(x) - U(x-l) \end{cases}, \tag{5}$$

$$\begin{cases} W^0(y) = W(y) - W(y-L) \\ U^0(y) = U(y) - U(y-L) \end{cases}, \tag{6}$$

where $l = D_3 - S_3 - S_4$ is the calculated trend length of the working face; $L = (D_1 - S_1 - S_2)\sin(\theta + \alpha)/\sin\theta$ is the calculated tendency length of the working face; D_3 is the trend length of the working face; D_1 is the tendency length of the working face; S_1, S_2, S_3, and S_4 are the inflection point displacements of the uphill, downhill, open off cut, and stop production line, respectively; and θ is the propagation angle of the mining influence.

In the case of limited mining, the subsidence and horizontal displacement of surface point A with coordinates are (x,y) along the direction of φ (the angle value from the positive counter-clockwise along the x axis to the specified direction) caused by the working face mining are as follows:

$$\begin{cases} W(x,y) = \frac{W^0(x)W^0(y)}{W_0} \\ U(x,y) = \frac{U^0(x)W^0(y)\cos\varphi + U^0(y)W^0(x)\sin\varphi}{W_0} \end{cases}. \tag{7}$$

By analyzing a large amount of measured data in mining areas, the BPM can predict the surface deformation caused by working face mining under different mining conditions, whether it is insufficient mining, full mining, or super full mining.

Exponent Knothe time function

The EKTF is based on the assumption that the subsidence speed of surface point A at time t is proportional to the difference between the final subsidence of this point and the instantaneous subsidence at time t (Chen et al. 2018):

$$\frac{dW(x,y,t)}{dt} = c\left[W(x,y) - W(x,y,t)\right], \tag{8}$$

where $dW(x,y,t)/dt$ is the subsidence speed of surface point A at time t; c is the time influence coefficient, which is related to the mining conditions of the working face and the characteristics of the overlying strata; and $W(x, y, t)$ is the subsidence of surface point A at time t.

According to the initial time condition $t = 0$ and $W(x,y,t) = 0$, the equation for calculating the instantaneous subsidence of surface point A can be obtained by integrating Eq. (8):

$$W(x,y,t) = W(x,y)(1 - e^{-ct}). \tag{9}$$

The curves of subsidence, subsidence speed, and subsidence acceleration with time in Eq. (9) are shown in Fig. 1a–c. It can be observed that when Eq. (9) is used to express the process of surface subsidence, it does not conform to the law of surface subsidence: (1) the subsidence speed gradually reaches the maximum subsidence speed, and then decreases from the maximum subsidence speed to 0; (2) the subsidence acceleration experiences the

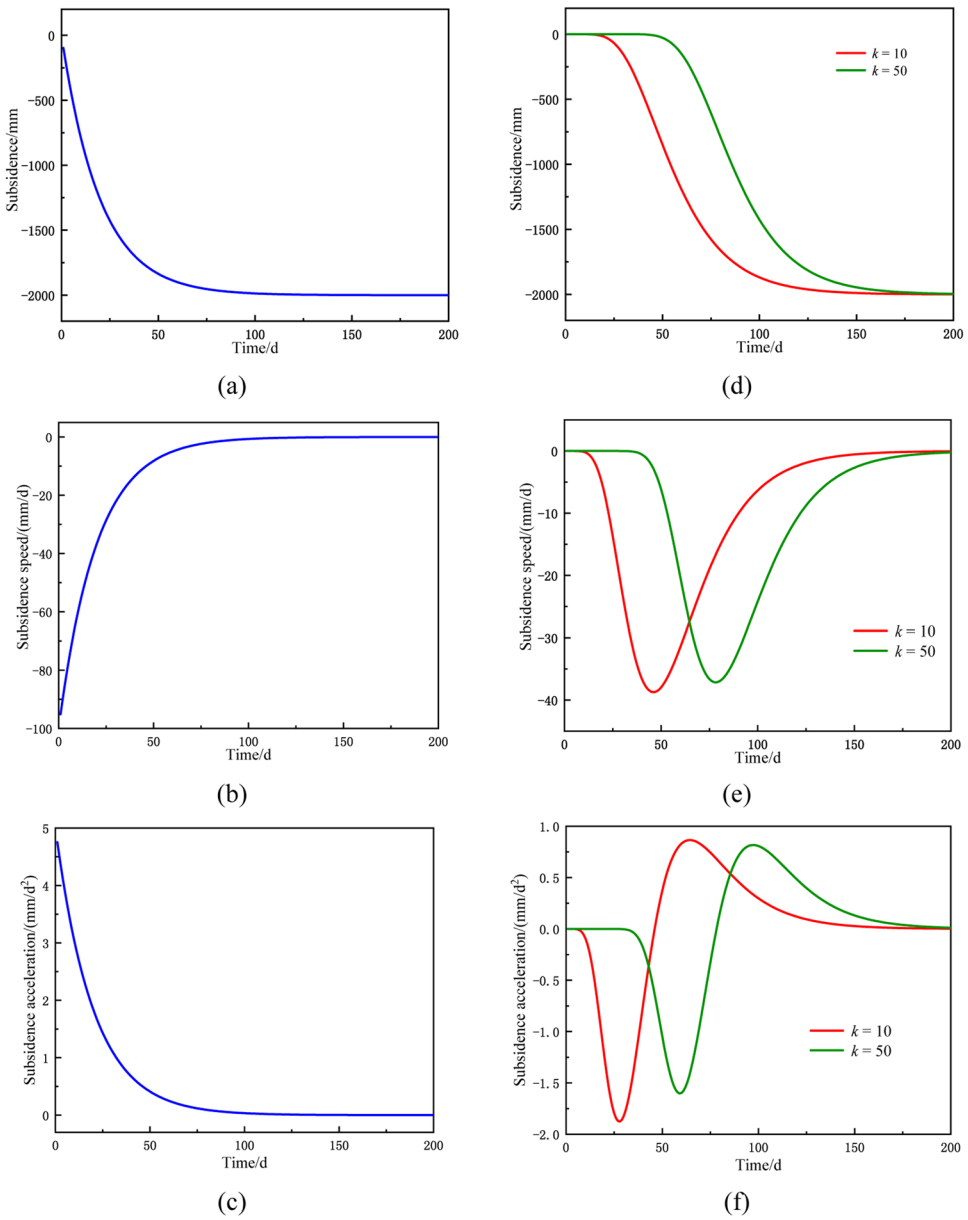

Fig. 1 Subsidence, subsidence speed, and subsidence acceleration with time

process from 0 to maximum subsidence acceleration and then back to 0; thereafter, it goes through the process from 0 to minimum subsidence acceleration and then back to 0.

To improve the applicability and reliability of Eq. (9) in the surface subsidence prediction, an exponent is added to control the subsidence acceleration. The EKTF equation is as follows:

$$W(x,y,t) = W(x,y)(1-e^{-ct})^{k} = W(x,y)f(t), \tag{10}$$

where k is the parameter related to the lithology of overlying strata.

The curves of the EKTF subsidence, subsidence speed, and subsidence acceleration change with time, as shown in Fig. 1d–f. It can be found that the EKTF can properly describe the above surface subsidence.

Model building

As a static prediction model, the BPM can predict the final surface deformation caused by working face mining. Because the subsidence of surface points is gradual process, the maximum deformation of the surface points is not instantaneously attained. Therefore, the dynamic prediction of surface deformation should be carried out in combining it with the time function, so as to obtain the deformation of the surface point in the process of subsidence.

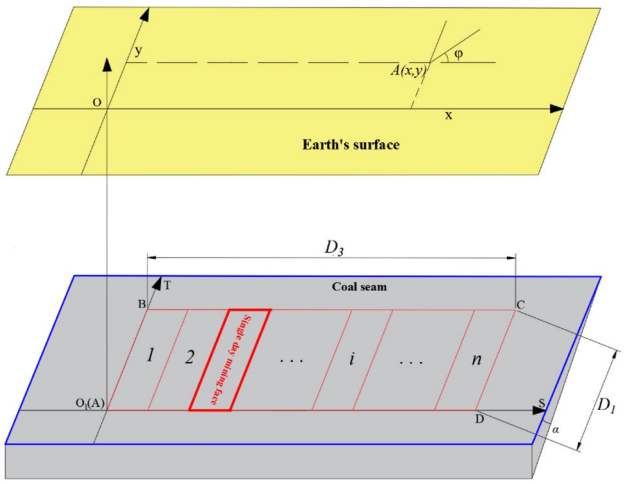

Fig. 2 Schematic diagram of working face division principle

As shown in Fig. 2, the working face is divided along the mining direction of the working face by a single-day mining face as a unit. Assuming that the average mining speed of the working face is v(m/day) daily, according to the principle of mining subsidence prediction, the coordinate of surface point A relative to the single-day mining face mined on day i is $(x\text{-}vi+v,y)$. Then, the final subsidence of surface point A caused by the single-day mining face mined on day i is as follows:

$$W(x,y,i)=\frac{W^0(x-vi+v)W^0(y)}{W_0}. \tag{11}$$

The final subsidence obtained by the BPM is combined with EKTF, considering that the influence time of the single-day mining face mined on day i for the surface point is t–i day. The subsidence of surface point A on day t caused by a single-day mining face mined on day i is as follows:

$$W(x,y,i,t)=W(x,y,i)f(t-i). \tag{12}$$

In a period of time after the mining of the working face is completed, the surface deformation caused by mining is still in the process of change; thus, the surface prediction is divided into the following two cases:

1. The mining of the working face is not completed entirely: when calculating the subsidence on day t, according to the principle of dynamic prediction mining time, the single-day mining face mined on day t does not affect the surface points, and only the previous t day needs to be considered. Therefore, the subsidence of surface point A on day t is obtained as follows:

$$W(x,y,t)=\sum_{i=0}^{t-1}W(x,y,i)f(t-i). \tag{13}$$

And the horizontal displacement of surface point A along the direction of φ on day t is obtained as follows:

$$U(x,y,t)=\sum_{i=0}^{t-1}U(x,y,i)f(t-i), \tag{14}$$

$$U(x,y,i)=\frac{U^0(x-vi+v)W^0(y)\cos\varphi+U^0(y)W^0(x-vi+v)\sin\varphi}{W_0}. \tag{15}$$

2. Mining of the working face has been completed: at this time, all single-day mining working faces will affect the surface points. Thus, the subsidence of surface point A on day t can be obtained as follows:

$$W(x,y,t)=\sum_{i=0}^{T}W(x,y,i)f(t-i), \tag{16}$$

where T is the total time required for the working face to complete the mining.

In addition, the horizontal displacement of surface point A along the direction of φ on day t is obtained as follows:

$$U(x,y,t)=\sum_{i=0}^{T}U(x,y,i)f(t-i) \tag{17}$$

In conclusion, the parameter system of the BPM-EKTF mining subsidence prediction model is $B=[q, \tan\beta, b, \theta, S_1, S_2, S_3, S_4, c, k]$.

Parameters solution

The BPM-EKTF mining subsidence prediction model is highly nonlinear, and its parameter solving is a significant problem. As a new swarm intelligence algorithm proposed in the recent years, the wolf pack algorithm not only solves the parameters of complex nonlinear problems and has appropriate robustness, but also has the advantages of strong global search ability and suitable local search ability and can easily jump out of the local optimal solution. It has been applied in many fields (Wu et al. 2013; Tian et al. 2020; Li et al. 2020a, b). Therefore, this paper introduces the wolf pack algorithm into the parameter solution of the BPM-EKTF mining subsidence prediction model, and the main solution process is as follows:

1. Fitness function construction: The measured surface subsidence and horizontal displacement were recorded as Wr and Ur, respectively. The predicted surface subsid-

ence and horizontal displacement obtained by the mining subsidence prediction model are recorded as *Ws* and *Us*, respectively. The number of measured subsidence and horizontal displacement points were recorded as *Nw* and *Nu*, respectively. The fitness function is constructed as follows:

$$F=\frac{\sum|Wr-Ws|}{Nw}+\frac{\sum|Ur-Us|}{Nu}. \tag{18}$$

2. Generation of wolves and head wolves: The perceived odor concentration of artificial wolves is evaluated based on the fitness function value. The smaller the fitness function value, the greater the perceived odor concentration of the artificial wolves. After a certain number of artificial wolves were produced, the artificial wolf with the highest odor concentration was selected as the head wolf.
3. Wandering behavior: Artificial wolves with high odor concentrations, except the head wolves, were selected as the exploring wolves. In the process of wandering, every exploring wolf searches for prey until its perceived odor concentration exceeds that of the head wolf, which is automatically promoted to the head wolf, ending the wandering behavior; otherwise, the behavior ends after reaching the maximum number of swimming. At the end of the wandering behavior, every exploring wolf moves forward to the position where the odor concentration is high.
4. Summoning behavior: Artificial wolves that are close to the head wolf were selected as fierce wolves. When the exploring wolves stop exploring, the head wolf summons the fierce wolves to approach itself. During the summoning process, if one of the fierce wolves perceives the odor concentration to exceed that of the head wolf, it will be automatically promoted to the head wolf. The summoning behavior will continue until the distance between every fierce wolf and the head wolf meets the distance requirement.
5. Besieging behavior: Considering the position of the head wolf as the assumed prey position, the fierce wolves cooperate with the detection wolves to attack the prey. During the siege, if one of the artificial wolves perceives an odor concentration that exceeds that of the lead wolf, the lead wolf is replaced by an artificial wolf. When the maximum number of sieges is reached, the besieging behavior ends.
6. Update of wolves: After the siege, some artificial wolves with low perceived odor perception concentration will be eliminated, and an equal number of artificial wolves will be randomly generated.
7. Steps (3)–(6) are repeated until the maximum number of cycles is reached, or the parameters of the mining subsidence prediction model meet the accuracy requirements, the cycles are broken, and the optimal solution is output.

Figure 3 shows the detailed flow of wolf pack algorithm to get the model parameters. Surface deformation was taken as the input measured data, according to the constructed fitness function, and the final parameters of mining subsidence prediction model were output as the results.

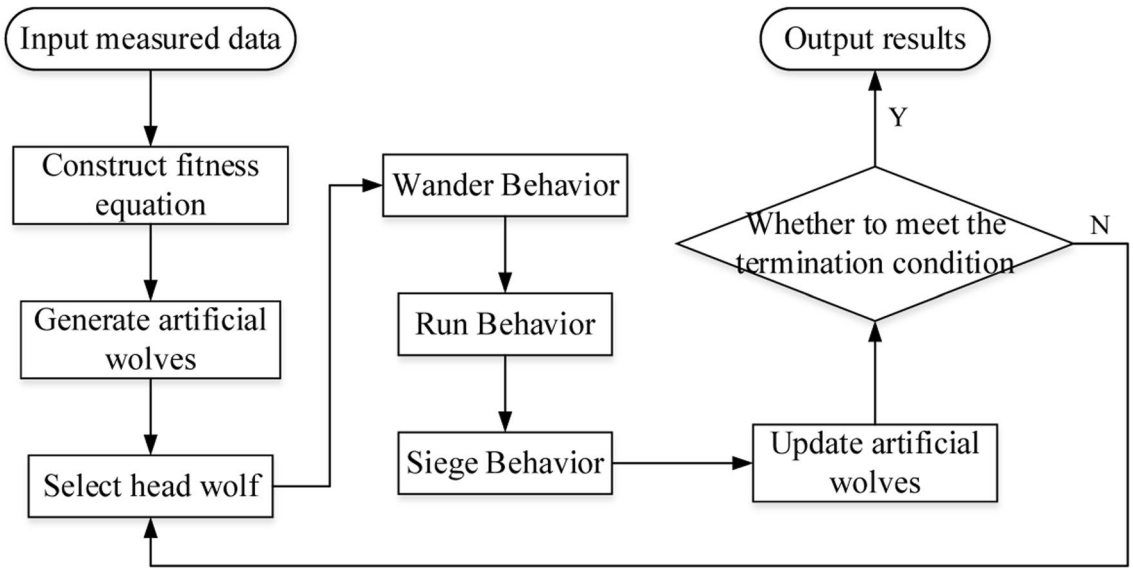

Fig. 3 Flow chart of model parameter solution

Application flow of mining subsidence monitoring model

The BPM-EKTF mining subsidence prediction model can obtain the surface deformation caused by working face mining for a certain time and space. When the relevant geological and mining conditions are known, the parameters of the model can be obtained according to the deformation of some surface points in time and space, and the deformation of any surface point in time and space can be obtained, provided that certain accuracy requirements are met. Accordingly, the TLS can be combined with the BPM-EKTF mining subsidence prediction model.

As shown in Fig. 4, the application flow of the mining subsidence monitoring method based on the BPM-EKTF and TLS is as follows:

1. Point cloud data acquisition: TLS is set at an appropriate location for point cloud data acquisition, such as concrete roads, hardened road centers, and other flat areas or close to trees, poles, buildings, and other areas with evident feature points. During single-station scanning, four or more target balls should be set near the TLS for coordinate transformation. The target balls should not be set along the same straight line.
2. Extraction of surface deformation: After preprocessing of point cloud data, such as filtering and denoising, a grid network of point cloud data is conducted. Taking the grid node as the feature point with the same name, the subsidence of the surface point is obtained by calculating the height difference of the feature point with the same name. The horizontal displacement is obtained by the plane coordinate difference between feature points with the same name.
3. Solution of model parameters: The BPM-EKTF mining subsidence prediction model is highly nonlinear, and its parameter solution is complicated. The wolf pack algorithm, which can be used in parameter solutions of nonlinear problems and has appropriate robustness, was applied to solve the model parameters.
4. Evaluation of parameter stability and accuracy: Contingency of parameter results was avoided using the wolf pack algorithm multiple times to solve the parameters. The mean square errors of the parameters were calculated to evaluate the stability of the parameter solution. The mean value of the results was taken as the final result, and the medium errors of fitting were calculated to evaluate the accuracy of the parameter solution.
5. Prediction and accuracy assessment of surface deformation: After the subsidence and horizontal displacement of the surrounding areas are obtained using the final results of the model parameters, the measured values of the horizontal observation station are compared with the predicted values. The medium and relative errors were calculated to evaluate the predicted accuracy.
6. Mining damage assessment to buildings: According to the predicted inclination, curvature, horizontal deformation, and mining damage grading table, a building mining damage assessment in the surrounding area was performed.

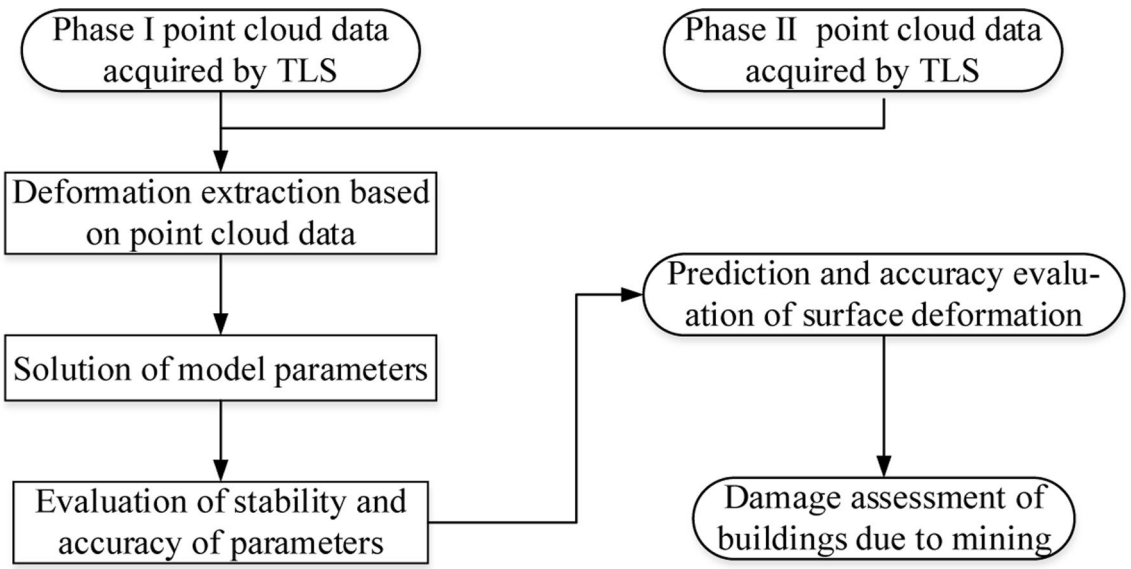

Fig. 4 Flow chart of monitoring model application

Area and data of application

Application area and data acquisition

In this study, the application area is the area surrounding the South 1312 (1) working face of Gubei Coal Mine, Huainan, and the TLS scanning area is the village on the left of the working face. The application area and TLS scanning data are displayed in the BJZ-54 geographic coordinate system, as shown in Fig. 5.

The South 1312 (1) working face was the first mining face of the Gubei Coal Mine, Huainan. The average mining thickness of the working face is 4.29 m, the inclination of the working face is 5°, and the average mining depth of the working face is 518 m. The entire working face adopts backward mining, mechanized tunneling, and all caving methods to manage the roof. The working face started mining on July 10, 2019 and was arranged along the coal seam strike. The average mining speed was 3.4 m/day. There are a large number of concrete roads without vegetation cover in the village on the left side of the working face, as well as numerous objects, such as residential buildings, telephone poles, and wood trees, on both sides of the road, providing the possibility for the TLS to obtain data and extract deformation.

The Zhong Haida HS-650 laser scanner, which adopts the pulse-type measurement method for ranging, was employed; the transmitter fires a laser at the object, and the laser is reflected on the object surface and then received by the receiver of the instrument. The scanner provides two laser pulse emission frequencies of 300 kHz (indoor) and 100 kHz (outdoor); the higher the frequency, the shorter the measurement distance. The range varies from 1.5 to 650 m. The scanning range was 0–360° horizontally and − 40° to 60° vertically. A ranging accuracy of 100 m can reach 5 mm. The TLS observation stations were arranged at a distance of 69 m from the open-cut eye. Multiple test stations were set along the direction of the working face. The distance between each station was 35 m, and the distance from the cutting position increased in turn. As shown in Fig. 6, during single-station scanning, the scanner was placed at the center of the concrete road, and four target balls were placed nearby for coordinate conversion. Moreover, the point cloud data of building corners, hardened road intersections, street lamps, and tree trunks can be obtained within the scanning range.

Surface deformation extraction scheme

After the TLS completes the collection of point cloud data, the Zhong Haida HD-3LS-SCEN was used to filter the collected data and filter out the point cloud data irrelevant to concrete roads, roadside buildings, street lamps, and tree trunks (Chen et al. 2017; You et al. 2021). Then, the coordinate transformation of the point cloud data was performed. There is no need to splice the multistation data in the coordinate transformation. The point cloud data are directly converted to the BJZ-54 geographic coordinate system through coordinates of the target balls in the TLS station and those in the geodetic coordinate system obtained by GPS (Gu et al. 2020). Finally, the deformation of the two periods of the data was extracted.

During subsidence extraction, the subsidence can be extracted by the elevation difference of the feature point with the same name. The two phases of data are gridded, and a 0.5×0.5 m grid is constructed in the scanning area. The same grid is used to divide the two phases of the point cloud data, and grid nodes with the same plane coordinates (x, y) are used as the feature points with the same name. The point cloud is searched in the grid, and the height z of the

Fig. 5 Application area and data

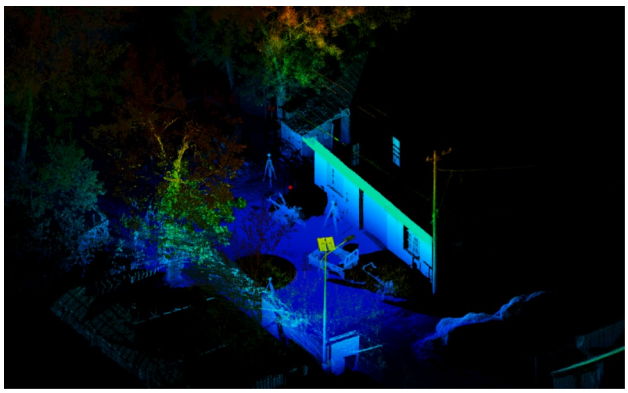

Fig. 6 Single-station scanning point cloud scene

feature points is provided according to the distance weighting to obtain the point subsidence.

The horizontal displacement is extracted based on the house feature points, road intersections, trees, and street lamp centers. For house feature points and road intersections, the plane coordinates are obtained by extracting the average value multiple times. For the center of trees and street lights, the plane coordinates at the relative height are obtained by implementing the least square method. Finally, the horizontal displacement of the two periods of data was extracted by the difference in plane coordinates.

The working face was not mined at the time when the point cloud data acquired by the TLS on July 9, 2019, was taken as the first observation data. However, the working face was mined when the point cloud data on October 25 of the same year was taken as the second observation data. Additionally, the surface deformation caused by mining was not stable. Table 1 presents the deformation of the two periods of data extracted according to the above scheme.

Results and analysis of application

Parameter solution results and analysis

Based on the subsidence and horizontal displacement extracted from the point cloud data, the wolf pack algorithm is used to solve the parameters of the prediction model. The algorithm was run four times to improve the validity, and the average value and mean square errors of the parameters were calculated, as shown in Table 2. Taking the mean value of multiple running results as the final result, the comparison between the deformation curve obtained by the prediction model and that obtained by the TLS is shown in Fig. 7.

Table 2 shows that the mean square errors of q, $\tan\beta$, B, and θ are controlled within 0.02, 0.03, 0.01, and 0.72°, respectively; the mean square errors of S, k, and c do not exceed 4.16 mm, 0.40, and 0.02, respectively. As shown in Fig. 7, the fitting value is approximately equal to the measured value of the TLS, and the variation trend is consistent. The absolute errors between the fitting and measured value of subsidence and horizontal displacement did not exceed 30 mm and 5 mm, respectively. In conclusion, using the point cloud data obtained by the TLS as the experimental data, the BPM-EKTF mining subsidence prediction model parameters obtained by the wolf pack algorithm are stable and accurate.

Prediction results and accuracy evaluation

Coal contributes to nearly 70% of China's natural energy. In recent years, the proportion of coal resources in energy consumption has gradually decreased, but it is still difficult to replace it in the short term. Coal resources are widely used,

Table 1 Surface deformation extraction results

Observation point number	Subsidence	Horizontal displacement	Observation point number	Subsidence	Horizontal displacement
1	− 633.25	716.29	11	− 864.62	
2	− 672.25		12	− 885.47	871.21
3	− 691.17		13	− 906.75	
4	− 708.54	767.73	14	− 946.25	
5	− 745.69		15	− 969.00	911.88
6	− 765.52	803.67	16	− 1014.28	
7	− 785.33		17	− 1081.79	958.48
8	− 804.69		18		999.96
9	− 824.27		19		1026.20
10	− 844.32	849.31	20		1031.79

Table 2 Results of parameter solution in application

Parameter	Average value	Mean square error	Parameter	Average value	Mean square error
q	1.109	0.018	S_2/m	47.432	3.466
$\tan\beta$	1.802	0.022	S_3/m	− 7.272	2.180
B	0.324	0.003	S_4/m	− 19.972	4.157
θ/°	87.008	0.715	k	4.756	0.397
S_1/m	67.503	4.112	c	0.245	0.015

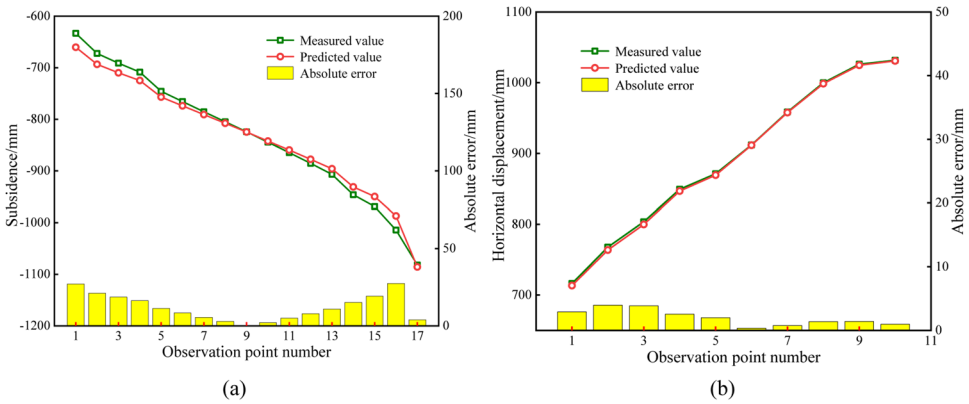

Fig. 7 Comparison of TLS measured deformation and fitting deformation

with a low cost, but coal mining is bound to cause strata displacement, deformation, and damage in the mining area.

To implement effective preventive measures in advance, it is necessary to accurately predict the influence scope of mining subsidence and the size of displacement and deformation (Kwinta and Gradka 2020; Ozdogan and Deliormanli 2020). The final results of the above parameter solution and working face parameters were substituted into the prediction model. The subsidence and horizontal displacement of the surrounding area were obtained, as shown in Fig. 8.

The accuracy of the predicted results was verified by comparing the predicted deformation of the observation station

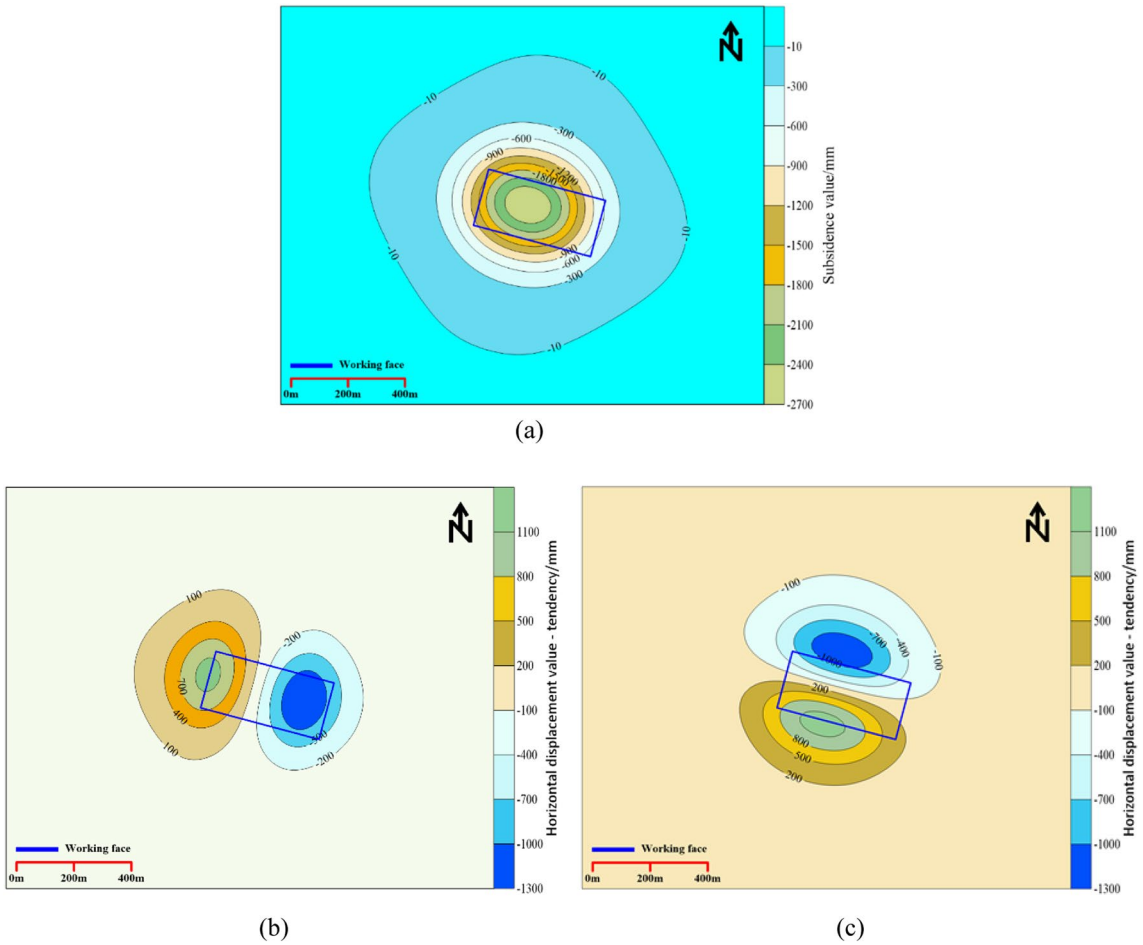

Fig. 8 General situation of subsidence and horizontal displacement: **a** Subsidence prediction figure; **b** and **c** Horizontal displacement prediction figure along the trend and tendency of working face, respectively

with the deformation measured by leveling. The obtained deformation comparison curves are shown in Fig. 9.

Figure 9 demonstrated that both the subsidence and horizontal displacement curves are consistent with the variation trend of the measured value of leveling. Except for the absolute error between the predicted value and the measured value of a few points between 100 and 170 mm, the absolute error between the predicted subsidence and the measured subsidence of the leveling is < 90 mm. The absolute error between the predicted horizontal displacement and the measured horizontal displacement of the leveling is < 80 mm. The absolute errors between the predicted and measured value of subsidence and horizontal displacement did not exceed 50 mm and 49 mm, respectively. The relative error of prediction was calculated as the ratio of the mean square error of prediction to the maximum deformation. The relative errors of prediction for subsidence and horizontal displacement were 2% and 5%, respectively. The mining subsidence monitoring method based on the BPM-EKTF and the TLS has high accuracy in the prediction of surface deformation.

Mining damage assessment of building

With the continuous mining of coal seams, the deformation of the overlying strata will spread to the surface, resulting in continuous or discontinuous deformation on the surface, often causing damage to buildings. As the main body of China's energy structure, coal mining for many years makes the contradiction between making full use of coal resources and protecting mining buildings increasingly acute. Therefore, it is necessary to assess the mining damage of buildings in the mining area to provide data support for protecting buildings around the mining area and provide the basis for determining the responsibility of building damage (Yang et al. 2018; Lian et al. 2020).

Based on the point cloud data obtained by the TLS, after point cloud data processing and deformation extraction, combined with the BPM-EKTF mining subsidence prediction model, the prediction figure of subsidence, inclination, and horizontal deformation of the surrounding surface caused by the mining of the working face on October 25, 2019 is drawn, as shown in Fig. 10. Because of the small curvature deformation, no deformation prediction figure was drawn.

Figure 10a illustrates that the villages on the left side and below the working face are affected by mining, and the closer the working face is, the greater is the mining impact. Most buildings on the left side of the working face are in the subsidence range of 10–300 mm, and a small part is in the subsidence range of 300–1500 mm, which is substantially affected by mining. The subsidence of most buildings in the villages below the working face is less than 10 mm, and only a small part of the buildings are located in the range of 10–300 mm, which is less affected by mining.

Figure 10b conveys that only a small portion of the buildings on the left side of the working face are in the inclined range of 2–8 mm/m, but most buildings are in the inclined range of 2–12 mm/m. The slope of the village buildings under the working face was small. Regardless of the trend inclination or tendency inclination, it was not more than 2 mm/m.

Figure 10c shows that only a small portion of the buildings near the working face in the village on the left side of the working face are in the horizontal deformation range of 2–8 mm/m, but nearly half of the buildings are in the horizontal deformation range of 2–7 mm/m. The horizontal deformation of the village buildings under the working face

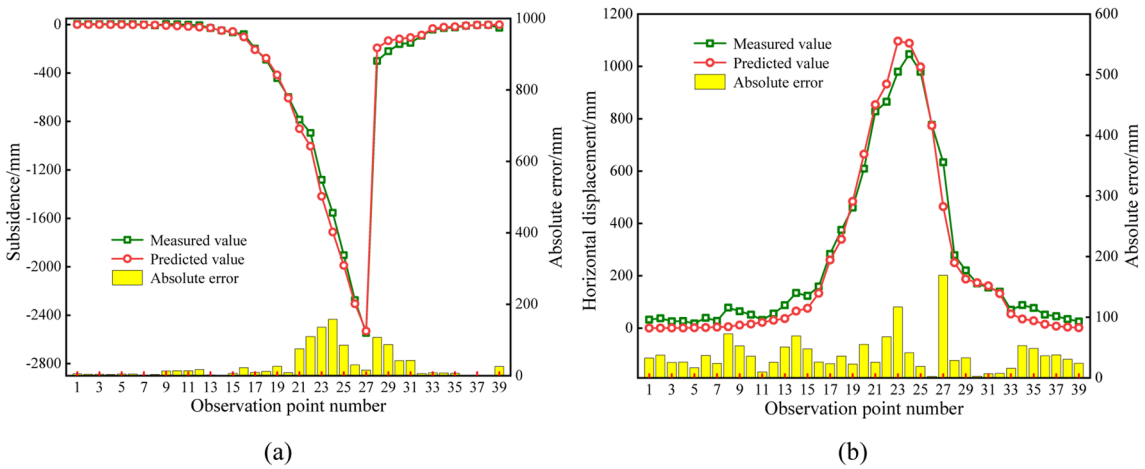

Fig. 9 Comparison of leveling measured deformation and predicted deformation

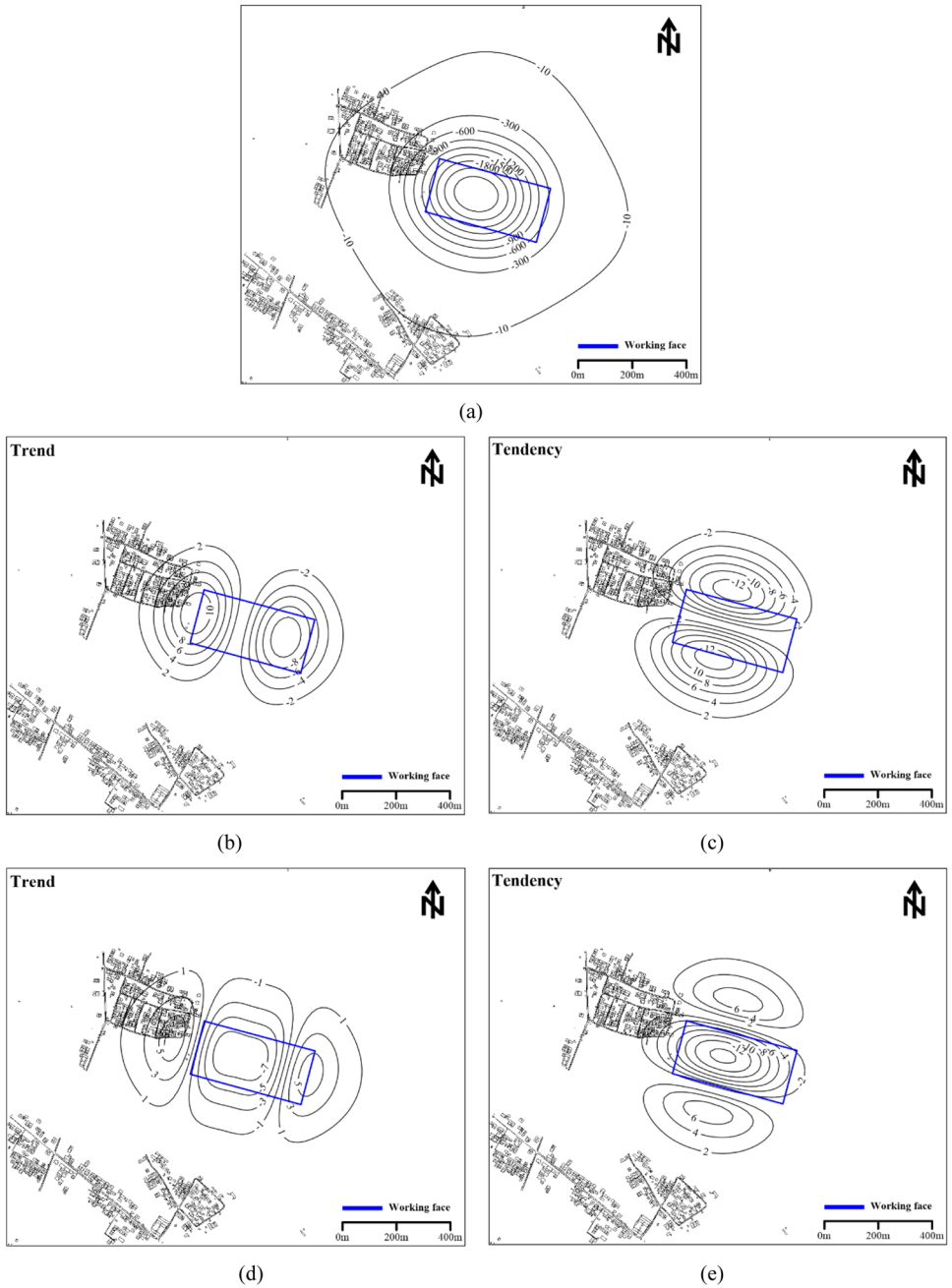

Fig. 10 Deformation prediction: **a** Subsidence prediction figure (unit: mm); **b**, **c** Inclined prediction figure along the trend and tendency of the working face, respectively (unit: mm/m); **d**, **e** Horizontal deformation prediction figure along trend and tendency of the working face, respectively (unit: mm/m)

is small, and the horizontal deformation of the trend and tendency is less than 2 mm/m.

The evaluation models and mining methods damage degree of surface buildings at home and abroad are based on a large number of field measurements and comprehensive analyses. In China, inclination K, curvature ε, and horizontal deformation i are used as damage classification indices. For brick concrete structure buildings with lengths less than 20 m, the damage level of buildings can be classified according to Table 3 (Cui et al. 2021). The application area in this study was located in the Gubei mining area, Huainan, China. The buildings affected by mining in the test area were concrete brick structures with a length of no more than 20 m. The structure of the mining damage classification is shown in Fig. 11.

From the beginning of working face mining (July 10, 2019) to October 25, 2019, the upper village close to the working face is greatly affected by mining. As a whole, the village buildings tend to be damaged more severely when they are closer to the cut-out of the working face. Owing to the distance from the working face, the villages below the working face are less affected by mining on the whole. Only a few buildings above the working face are rated as grade IV mining damage.

Table 3 Damage classification of brick concrete structure buildings

ε/mm/m	i/mm/m	$K/10^{-3}$/mm	Damage level	Structural treatment
≦2.0	≦3.0	≦0.2	I	No maintenance
				Simple maintenance
≦4.0	≦6.0	≦0.4	II	Minor maintenance
≦6.0	≦10.0	≦0.6	III	Medium maintenance
> 6.0	> 10.0	> 0.6	IV	Major maintenance
				Demolition and construction

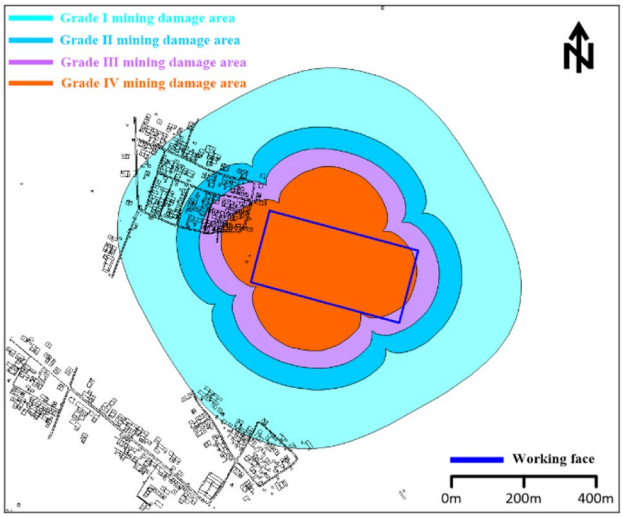

Fig. 11 Classification of building mining damage

In the grade IV damage area of the village above the working face, two residential houses were randomly visited. Cracks were found on the walls of the residential houses (as shown in Fig. 12), and the houses appeared to have collapsed, causing a severe threat to the production and life of the residents.

Discussion

Comparison of mining subsidence monitoring model

The PIM (Xia and Wang 2020) is based on the random medium theory of strata movement. The normal distribution function is used as the influence function, and the integral expression is used to express the subsidence influence basin. Owing to its mature theory, the PIM has become a static prediction method for mining subsidence designated by the Chinese government. The KTF (Guzy and Malinowska 2020) is based on the assumption that the subsidence speed at a particular time is proportional to the difference between the final subsidence and instantaneous subsidence at that time. This time function has a few parameters and is widely used to describe the process of surface subsidence (Gruszczynski et al. 2019).

To explore the applicability of the BPM-EKTF and PIM-KTF mining subsidence prediction models in combination with the TLS for surface monitoring, this study uses the point cloud data obtained by the TLS as the experimental data and the measured leveling data of the observation station as the comparative data. Finally, the prediction results are obtained, as shown in Fig. 13.

Figure 13 depicts that the absolute error of subsidence obtained by the PIM-KTF is in the range of 0–300 mm, and

Fig. 12 Cracks in damaged buildings

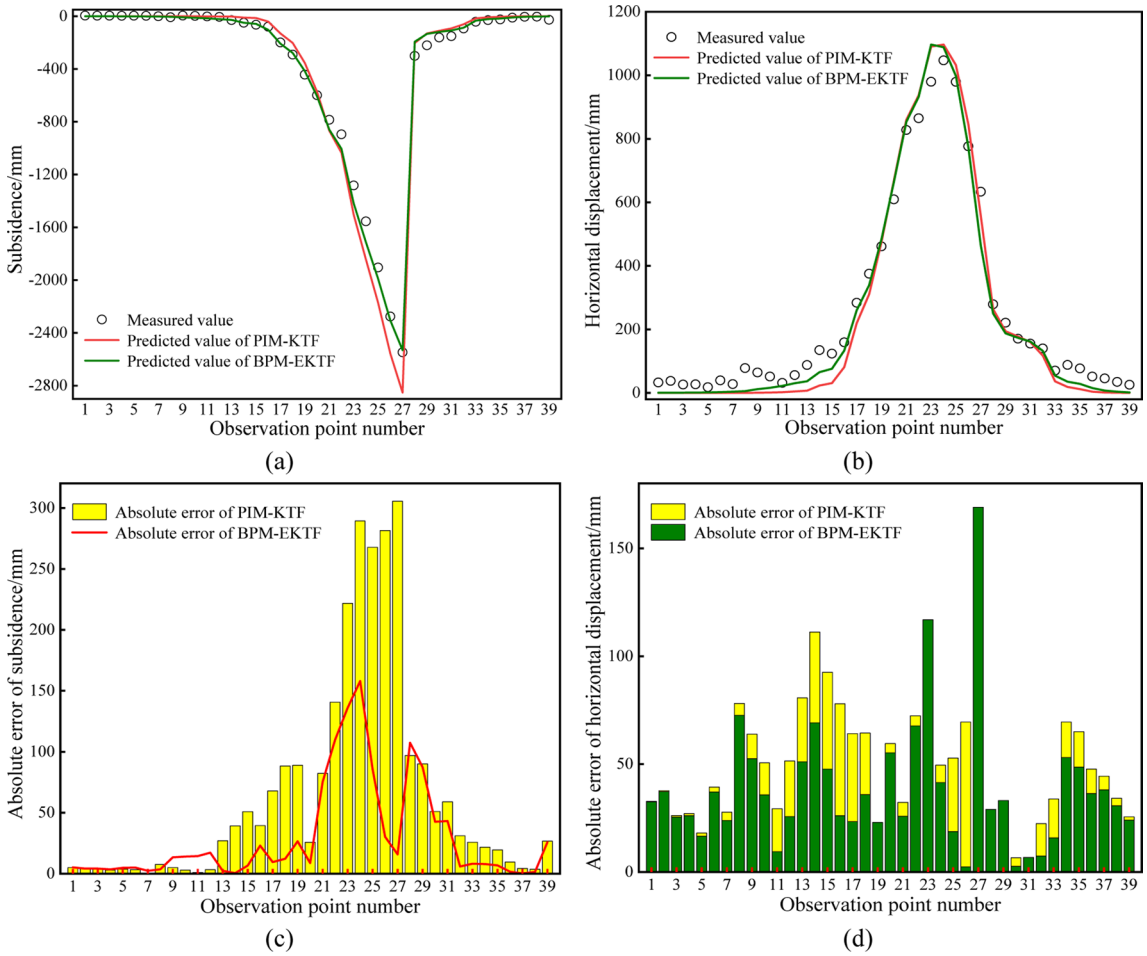

Fig. 13 Comparison of predicted results of BPM-EKTF and PIM-KTF

the absolute error of horizontal displacement is in the range of 0–150 mm. The absolute error of subsidence obtained by the BPM-EKTF is in the range of 0–200 mm, and the absolute error of the horizontal displacement is in the range of 0–200 mm. However, the absolute error histogram shows that the absolute error of the horizontal displacement of individual observation stations is slightly larger, which leads to the upper limit of the absolute error interval of horizontal displacement obtained by the BPM-EKTF being slightly larger than that of the PIM-KTF. Through calculation, the mean square error of subsidence and horizontal displacement of the PIM-KTF is 109 mm and 56 mm, respectively, and those of the BPM-EKTF is 50 mm and 49 mm, respectively. Overall, the predicted effect of the BPM-EKTF combined with the TLS was better than that of the PIM-KTF.

Ability of antigeological mining condition error

The structure of the overlying strata in the gob is complex, including a large number of structural planes, such as faults and joints (Kryzia et al. 2018; Suganthi and Elango 2020; Lyros et al. 2021). With the continuous mining of the working face, the structure and properties of the rock stratum are constantly changing. Although much research has been conducted on the influence law of various geological and mining conditions, it is still unable to accurately and reliably obtain the geological and mining conditions at any time of mining.

The resistance of the mining subsidence detection method based on the TLS and BPM-EKTF to the error of geological mining conditions was verified through the design of the following experiments: Based on the geological mining conditions of the working face in the application, the original values of m, α, and H vary together, and the change ranges are -20%, -10%, 10%, and 20%, respectively. After each change, the parameters of the mining subsidence prediction model were calculated four times, and the mean value was taken as the final result. The deformation of the observation station was predicted and compared with the measured leveling value. The comparison results are shown in Fig. 14.

As shown in Fig. 14, the changing trend of the predicted value of the observation station is consistent with the measured value, and the absolute error of subsidence and

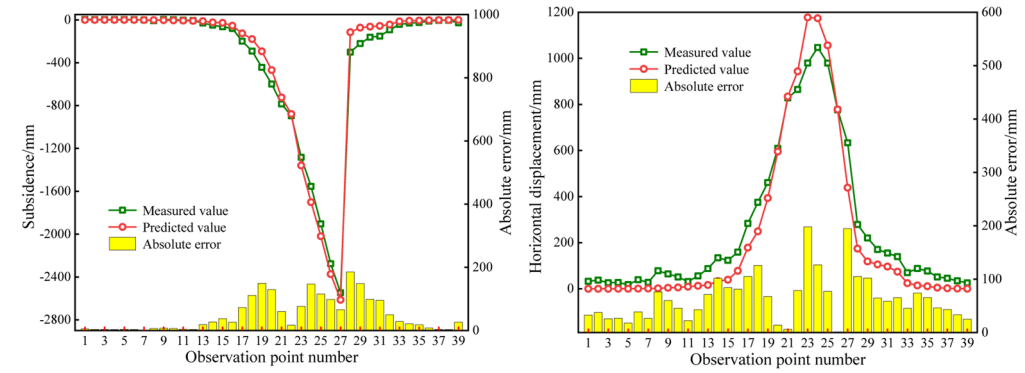

(a) -20%

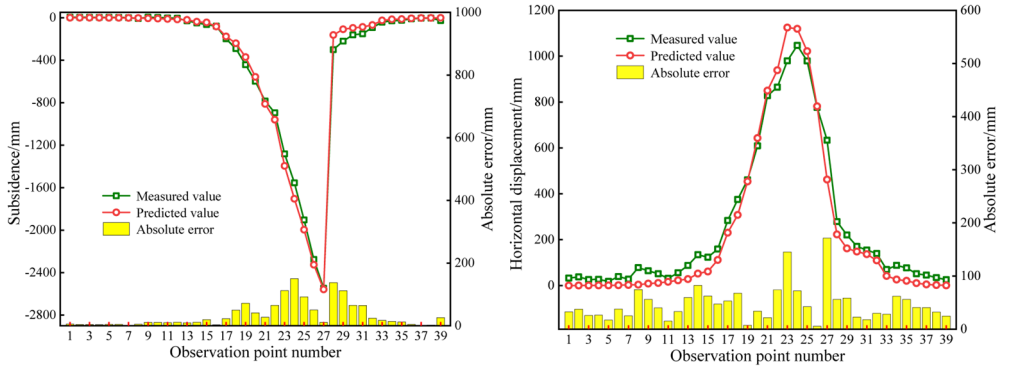

(b) -10%

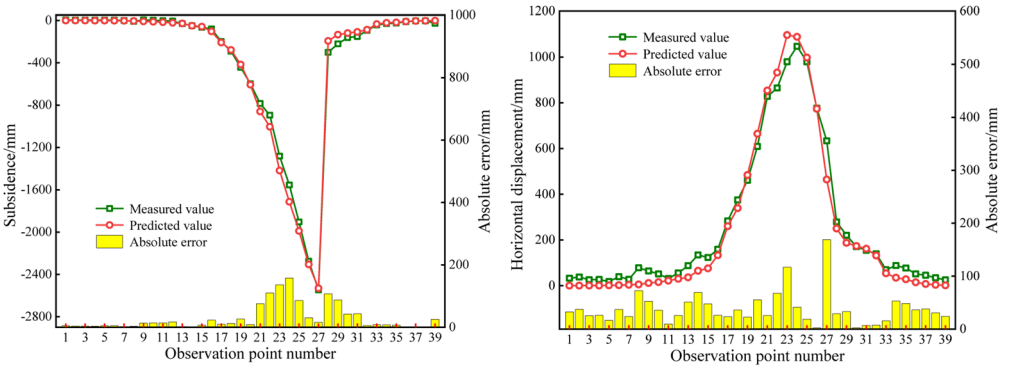

(c) 0%

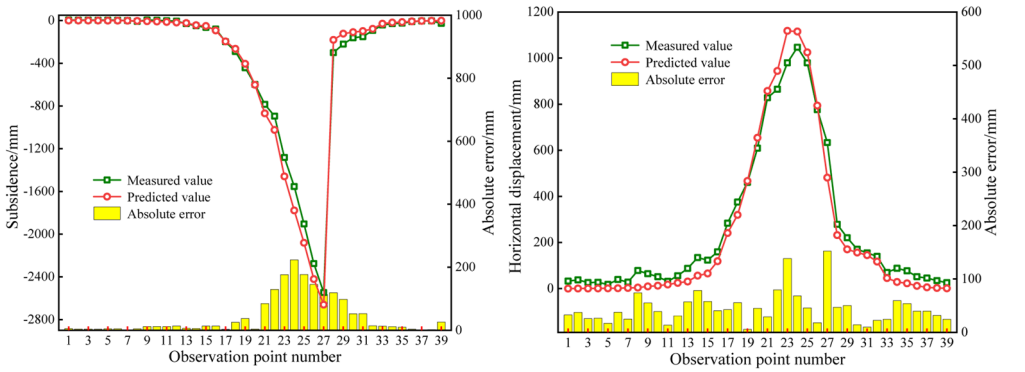

(d) +10%

Fig. 14 Result of antigeological mining condition error

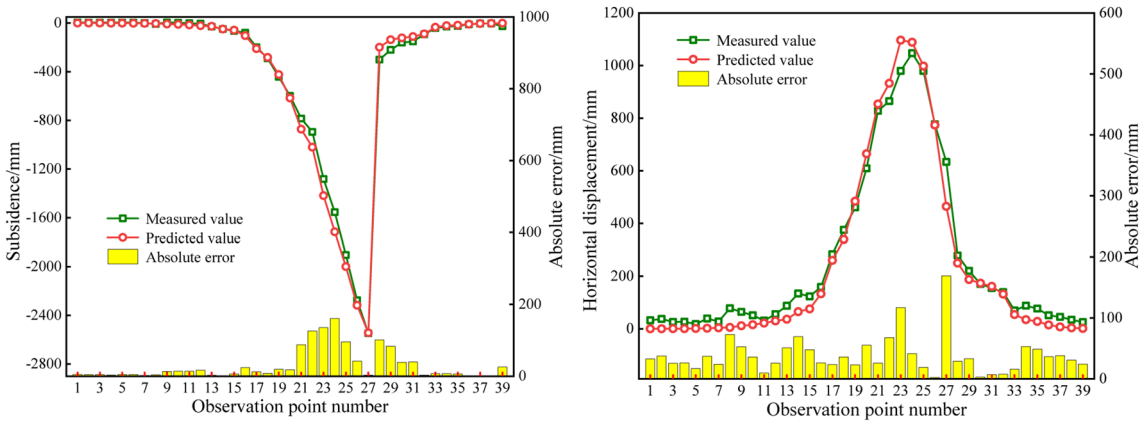

(e) +20%

Fig. 14 (continued)

horizontal displacement were < 250 mm. In the vicinity of the observation station with maximum subsidence and horizontal displacement, the absolute error is large; the closer to the maximum deformation point, the larger the absolute error. However, it was found that with the change in geological and mining conditions, this trend did not change significantly. After the original values of m, α, and H are changed, the mining subsidence monitoring method based on the BPM-EKTF and TLS can still obtain relatively accurate and reliable surface deformation and has resistance to errors in geological and mining conditions.

Conclusion

In this study, the BPM-EKTF mining subsidence prediction model was constructed to describe the surface deformation caused by mining, and a mining subsidence monitoring method based on the BPM-EKTF and TLS was proposed and applied to the building mining damage assessment in the surrounding area of the working face. After using TLS to carry out small-scale observation on the area with roads, trees, buildings and other characteristic objects, combined with the mining subsidence prediction model constructed in this paper, the surface deformation caused by mining in a wide range of areas can be obtained. The results of this work can provide a reference for predicting mining subsidence influence scope, deformation size, and mining damage assessment of mining buildings. The main conclusions are as follows:

1. According to the subsidence and horizontal displacement of a few discrete points extracted from the TLS scanning point cloud data, the parameters of the BPM-EKTF mining subsidence prediction model were obtained using the wolf pack algorithm. The results show that the mean square errors of q, $\tan\beta$, B, and θ are controlled within 0.02, 0.03, 0.01, and 0.72°, respectively; the mean square errors of S, k, and c do not exceed 4.16 mm, 0.40, and 0.02, respectively. The absolute errors between the fitting and measured value of subsidence and horizontal displacement did not exceed 30 mm and 5 mm, respectively. The BPM-EKTF surface prediction model parameters obtained using this algorithm are stable and accurate.
2. After the model parameters were introduced into the BPM-EKTF mining subsidence prediction model, the subsidence and horizontal displacement of the surrounding area of the working face was obtained and compared with the measured leveling values of the observation station. The results show that the absolute errors between the predicted and measured value of subsidence and horizontal displacement did not exceed 50 mm and 49 mm, respectively. The relative errors of prediction for subsidence and horizontal displacement were 2% and 5%, respectively. The mining subsidence monitoring method based on the BPM-EKTF and TLS has high accuracy in predicting surface movement and deformation.
3. According to the predicted deformation, the mining damage to the buildings around the working face was evaluated. The results show that the villages on the left side and below the working face are affected by mining, and the closer the working face is, the greater is the mining impact. Overall, the village near the working face on the left is more affected by mining, while the village far away from the working face on the lower side is less affected by mining.
4. In the discussion, the applicability of the BPM-EKTF and PIM-KTF mining subsidence prediction models combined with the TLS for mining subsidence moni-

toring was compared. The results show that the mean square error of subsidence and horizontal displacement of the PIM-KTF is 109 mm and 56 mm, respectively, and those of the BPM-EKTF is 50 mm and 49 mm, respectively. The prediction effect of the BPM-EKTF combined with the TLS is better than that of the PIM-KTF.

5. The resistance ability of the mining subsidence monitoring method based on the BPM-EKTF and the TLS for geological mining condition error is discussed in the discussion. The results show that the changing trend of the predicted value of the observation station is consistent with the measured value, and the absolute error of subsidence and horizontal displacement were < 250 mm. The mining subsidence monitoring method combined with the BPM-EKTF and TLS is resistant to the geological mining condition error.

Acknowledgements The work was supported by the National Natural Science Foundation of China [Grant numbers 52074010, 41602357]. We would like to thank Dr. Chuang Jiang, Dr. Shenshen Chi, and all the surveyors involved in this project for delivering sufficient data.

Declaration

Conflict of interest The authors declare that they have no conflict of interest.

References

Bonneau DA, DiFrancesco PM, Hutchinson DJ (2020) A method for vegetation extraction in mountainous terrain for rockfall simulation. Remote Sens Environ 251:112098

Boscarino S, Cho SY, Russo G, Yun SB (2021) High Order conservative semi-lagrangian scheme for the BGK model of the Boltzmann equation. Commun Comput Phys 29(1):1–56

Chang ZQ, Wang JZ (2003) Study on time function of surface subsidence—the improved knothe time function. Chin J Rock Mech Eng 09:1496–1499 (**in Chinese**)

Chen YF, Zha JF, Xu MQ, Zhang ZH, Li JL (2017) Center line extraction of road street light pole point cloud core line in mining area. Coal Eng 49(03):111–114 (**in Chinese**)

Chen L, Zhao XS, Tang YX, Zhang H (2018) Parameters fitting and evaluation of exponent Knothe model combined with InSAR technique. Rock Soil Mech 39(S2):423–431 (**in Chinese**)

Cui XM, Che YH, Zhao YL, Li PX, Bai ZH (2021) Rediscussions on the mining deformation and the building damage classification. J China Coal Soc 46(01):145–153 (**in Chinese**)

Cwiakala P, Gruszczynski W, Stoch T, Puniach E, Mrochen D, Matwij W, Matwij K, Nedzka M, Sopata P, Wojcik A (2020) UAV applications for determination of land deformations caused by underground mining. Remote Sens 12(11):25

Gruszczynski W, Niedojadlo Z, Mrochen D (2019) Uncertainty in determining the parameters of the surface deformation model. Acta Geodynamica Et Geomaterialia 16(2):211–218

Gu YY, Zhou DW, Zhang DM, Wu K, Zhou BH (2020) Study on subsidence monitoring technology using terrestrial 3D laser scanning without a target in a mining area: an example of Wangjiata coal mine, China. Bull Eng Geol Environ 79(7):3575–3583

Guzy A, Malinowska AA (2020) Assessment of the impact of the spatial extent of land subsidence and aquifer system drainage induced by underground mining. Sustainability 12(19):7871

Jiang Y, Misa R, Sroka A, Jiang Y (2021) Mitigating land subsidence damage risk by Fly Ash Backfilling Technology: an injection case in overburden of coal mining. Pol J Environ Stud 30(1):655–661

Kryzia K, Majcherczyk T, Niedbalski Z (2018) Variability of exploitation coefficient of knothe theory in relation to rock mass strata type. Arch Min Sci 63(3):767–782

Kumar S, Kumar D, Chaudhary SK, Singh N, Malik KK (2020) Land subsidence mapping and monitoring using modified persistent scatterer interferometric synthetic aperture radar in Jharia Coalfield, India. J Earth Syst Sci. https://doi.org/10.1007/s12040-020-01413-0

Kwinta A, Gradka R (2020) Analysis of the damage influence range generated by underground mining. Int J Rock Mech Min Sci 128:9

Li HB, Yang XG, Sun HL, Qi SC, Zhou JW (2019) Monitoring of displacement evolution during the pre-failure stage of a rock block using ground-based radar interferometry. Landslides 16(9):1721–1730

Li LP, Cui LY, Liu HL, Qin CS, Hu J, Zhang MG (2020a) A method of tunnel critical rock identification and stability analysis based on a laser point cloud. Arab J Geosci 13(13):10

Li JY, Wang L, Zhu SJ, Teng CQ, Jiang KG (2020b) Research on parameters estimation of probability integral model based on wolves pack algorithm. China Mining Magazine 29(10):102–109 (**in Chinese**)

Lian XG, Dai HY, Ge LL, Cai YF (2020) Assessment of a house affected by ground movement using terrestrial laser scanning and numerical modeling. Environ Earth Sci 79(9):10

Liu H, Deng K, Zhu X, Jiang C (2019) Effects of mining speed on the developmental features of mining-induced ground fissures. Bull Eng Geol Environ 78(8):6297–6309

Lyros E, Kostelecky J, Plicka V, Vratislav F, Sokos E, Nikolakopoulos K (2021) Detection of tectonic and crustal deformation using GNSS data processing: the case of PPGnet. Civ Eng J 7(1):14–23

Malinowska A, Hejmanowski R, Dai HY (2020) Ground movements modeling applying adjusted influence function. Int J Min Sci Technol 30(2):243–249

Monmarche P (2021) A note on Fisher information hypocoercive decay for the linear Boltzmann equation. Anal Math Phys. https://doi.org/10.1007/s13324-020-00437-5

Ozdogan MV, Deliormanli AH (2020) Determination of possible failure surfaces in an open-pit slope caused by underground production. Bollettino Di Geofisica Teorica Ed Applicata 61(2):199–218

Suganthi S, Elango L (2020) Estimation of groundwater abstraction induced land subsidence by SBAS technique. J Earth Syst Sci 129(1):13

Tian J, Zhao J, Zhou W, Han X, Wang L (2020) A wolf pack optimization theory based improved density peaks clustering approach. Tehnicki Vjesnik-Technical Gazette 27(6):1910–1916

Vos S, Spaans L, Reniers A, Holman R, McCall R, de Vries S (2020) Cross-shore intertidal bar behavior along the Dutch coast: laser measurements and conceptual model. J Mar Sci Eng 8(11):864

Wang YP, Xiong LX (2020) Numerical analysis of the influence of bolt set on the shear resistance of jointed rock masses. Civ Eng J 6(6):1039–1055

Wang N, Wu K, Liu J, An SK (2013) Model for mining subsidence prediction based on Boltzmann function. J China Coal Soc 38(08):1352–1356 (**in Chinese**)

Wang BL, Xu JL, Xuan DY (2018) Time function model of dynamic surface subsidence assessment of grout-injected overburden of a coal mine. Int J Rock Mech Min Sci 104:1–8

Wojtkowska M, Kedzierski M, Delis P (2021) Validation of terrestrial laser scanning and artificial intelligence for measuring deformations of cultural heritage structures. Measurement 167:108291

Wu HS, Zhang FN, Wu LS (2013) New swarm intelligence algorithm—wolf pack algorithm. Syst Eng Electron 35(11):2430–2438 (**in Chinese**)

Xia Y, Wang Y (2020) InSAR- and PIM-based inclined Goaf determination for illegal mining detection. Remote Sens 12(23):3884

Xiao L, Bi Y, Du S, Wang Y, Guo C, Christie P (2021) Response of ecological stoichiometry and stoichiometric homeostasis in the plant-litter-soil system to re-vegetation type in arid mining subsidence areas. J Arid Environ 184:104298

Xing X, Zhu Y, Yuan Z, Xiao L, Liu X, Chen L, Xia Q, Liu B (2021) Predicting mining-induced dynamic deformations for drilling solution rock salt mine based on probability integral method and weibull temporal function. Int J Remote Sens 42(2):639–671

Yang ZF, Li ZW, Zhu JJ, Preusse A, Hu J, Feng GC, Wang YJ, Papst M (2018) An InSAR-based temporal probability integral method and its application for predicting mining-induced dynamic deformations and assessing progressive damage to surface buildings. IEEE J Select Topics Appl Earth Observ Remote Sens 11(2):472–484

Yao WZ, Xu KK, Liu JP, Shao ZH, Zhu XL (2021) Surface subsidence monitoring in mining area based on dislocation model. Sci Surv Mapping 46(03):32–39 (**in Chinese**)

You L, Guo J, Pang Y, Tang S, Song X, Zhang X (2021) 3D stem model construction with geometry consistency using terrestrial laser scanning data. Int J Remote Sens 42(2):714–737

Yuan L, Jiang YD, Wang K, Zhao YX, Hao XJ, Xu C (2018) Precision exploitation and utilization of closed/abandoned mine resources in China. J China Coal Soc 43(01):14–20 (**in Chinese**)

Zeng Q, Shen L, Yang J (2020) Potential impacts of mining of superthick coal seam on the local environment in arid Eastern Junggar coalfield, Xinjiang region, China. Environ Earth Sci 79(4):15

Zhu X, Guo G, Liu H, Yang X (2019) Surface subsidence prediction method of backfill-strip mining in coal mining. Bull Eng Geol Env 78(8):6235–6248